Sm-Fe-N 系磁石の磁気特性

齋藤哲治
（千葉工業大学）

Magnetic properties of Sm-Fe-N magnets

Tetsuji Saito
(Chiba Institute of Technology)

はじめに

Sm-Fe-N 合金粉末は高温で分解するため Nd-Fe-B 磁石とは異なり、焼結により固化成形できないことが欠点となっていた。そのため、現在 Sm-Fe-N 磁石はボンド磁石として使用されている。最近、新しい固化成形法として Nd-Fe-B アモルファス合金粉末などをアモルファスのまま固化成形できる冷間圧縮せん断法が開発された。この冷間圧縮せん断法は冷間で粉末を圧縮せん断することを特徴とする[(1)]。そのため、高温で分解する Sm-Fe-N 合金粉末も冷間圧縮せん断法により固化成形できることがわかってきた[(2)]。しかし、冷間圧縮せん断法では板状の試料しか作製できない。そこで、放電プラズマ焼結法により Sm-Fe-N 合金粉末が固化成形できるかどうかについて検討したところ、高温で分解する Sm-Fe-N 合金粉末も放電プラズマ焼結法により固化成形できることがわかってきた。本研究では放電プラズマ焼結法により作製した Sm-Fe-N 磁石の磁気特性について調べたので報告する。

実験方法

原料粉末して $TbCu_7$ 型および Th_2Zn_{17} 型の 2 種類の Sm-Fe-N 合金粉末を用いた。まず、これらの Sm-Fe-N 合金粉末の固化成形を冷間圧縮せん断法で試みた。なお、雰囲気は大気中、温度は室温で行った。次に Sm-Fe-N 合金粉末の固化成形を放電プラズマ焼結法で試みた。なお、焼結条件としては、雰囲気は真空中、焼結温度は 673－873K、焼結圧力は 100MPa とした。得られた試料の密度はアルキメデス法で測定した。得られた試料の構造と組織は、X 線回折装置、走査型電子顕微鏡および EPMA で調べた。また得られた試料の熱磁気特性は振動試料型磁力計で、ヒステリシス曲線は振動試料型磁力計で測定した。

結果および考察

冷間圧縮せん断法では $TbCu_7$ 型および Th_2Zn_{17} 型の Sm-Fe-N 合金粉末ともほとんど分解することなくバルクの磁石に固化成形できることが、また得られた Sm-Fe-N 磁石は原料粉末と同様に高い磁気特性を示すことがわかった。しかし、放電プラズマ焼結法では Th_2Zn_{17} 型の Sm-Fe-N 合金粉末は低温でも一部分解してしまうことが、また高温（873K）では完全に分解してしまうことがわかった。それに対して、$TbCu_7$ 型の Sm-Fe-N 合金粉末も高温では完全に分解してしまうが、低温では分解することなく固化成形できることがわかった。

図 1 に $TbCu_7$ 型の Sm-Fe-N 合金粉末と放電プラズマ焼結法により作製した $TbCu_7$ 型の Sm-Fe-N 磁石のヒステリシス曲線を示す。放電プラズマ焼結法により作製した $TbCu_7$ 型の Sm-Fe-N 磁石は原料粉末とほぼ同等の高い磁気特性を示すことがわかった。

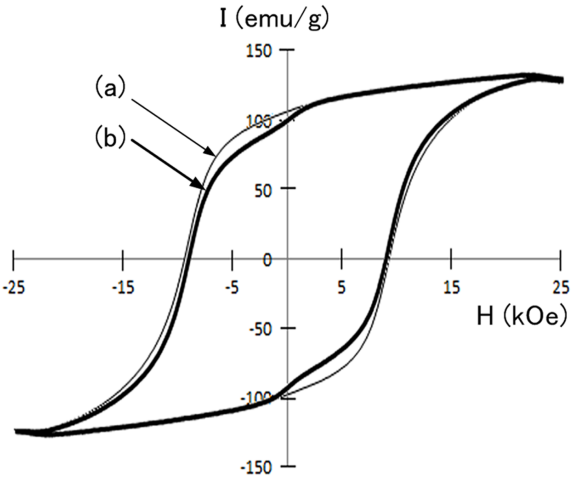

Fig.1 Hysteresis loops of (a) Sm-Fe-N powder and (b) Sm-Fe-N magnet produced by spark plasma sintering method.

参考文献

1) T. Saito, H. Takeishi, and N. Nakayama, J. Mater. Res., vol.20, No.3, pp.563-566 (2005).
2) T. Saito, H. Sato, H. Takeishi, and N. Nakayama, Appl. Phys. Lett. vol. 89, 162511 (2006).

面内磁気異方性を持つエピタキシャル RCo$_5$ 規則合金膜の構造解析

堀田裕介・山田真・鈴木中・大竹充・二本正昭・桐野文良*・稲葉信幸**
（中央大，*東京藝大，**山形大）

Structural Characterization of RCo$_5$ Ordered Alloy Epitaxial Thin Films with In-plane Magnetic Anistropies

Yusuke Hotta, Makoto Yamada, Ataru Suzuki, Mitsuru Ohtake,
Masaaki Futamoto, Fumiyoshi Kirino*, and Nobuyuki Inaba**
(Chuo Univ., *Tokyo Univ Arts, **Yamagata Univ.)

はじめに　希土類金属（R）と3d 強磁性遷移金属のCoからなるRCo$_5$ 規則合金は高いK_u 特性を示し，その薄膜は薄膜磁石，アクチュエータ，マイクロモータなどへの応用に向けた研究が行われている．これまで，(100)もしくは(211)配向のW[1]やCr[2]，Fe[3]などのbcc金属下地層を用いることにより，c軸が面内に存在するエピタキシャルSmCo$_5$膜の形成が報告されている．本研究では，MgO単結晶基板上にヘテロエピタキシャル成長させたCr(100)およびCr(211)下地層上に種々の希土類元素を用いたRCo$_5$規則合金膜の形成を行い，膜形成条件と膜構造の関係を調べた．

実験方法　膜形成には超高真空分子線蒸着装置を用いた．MgO(100)および MgO(110)基板上に，それぞれ，ヘテロエピタキシャル成長させた Cr(100)および Cr(211)下地層上に 20 nm 厚の R と Co の組成比が 1：5 となる組成で基板温度 500 °C で膜形成した. 構造評価にはRHEEDおよびXRD, 磁気特性評価には VSM を用いた．

実験結果　Fig. 1(a)および(b)に Cr(100)下地層上に Sm-Co 膜形成中に観察した RHEED パターンを示す．形成初期段階から製膜後まで，Fig. 1(d)の SmCo$_5$(11$\bar{2}$0)表面の形成を示す回折パターンが観察されており，エピタキシャル SmCo$_5$ 膜が得られていることが分かる．RHEED 解析により決定したエピタキシャル方位関係は以下の通りである．

SmCo$_5$(11$\bar{2}$0)[0001] || Cr(100)[011]
SmCo$_5$(11$\bar{2}$0)[1$\bar{1}$00] || Cr(100)[011]

SmCo$_5$ 膜は，c 軸が面内に存在し，互いに直交した方位関係を持つ 2 つのバリアントから構成されていることが分かった．Fig. 2 に XRD パターンを示す．面外パターンでは，SmCo$_5$(11$\bar{2}$0)反射が認められる．面内パターンでは，SmCo$_5$(0002)基本反射に加え，SmCo$_5$(0001)超格子反射も観察されており，RT_5 型構造に規則化した SmCo$_5$ 膜が形成されていることが分かる．当日は Sm 以外の R 元素を用いた RCo$_5$ 膜についても報告する．

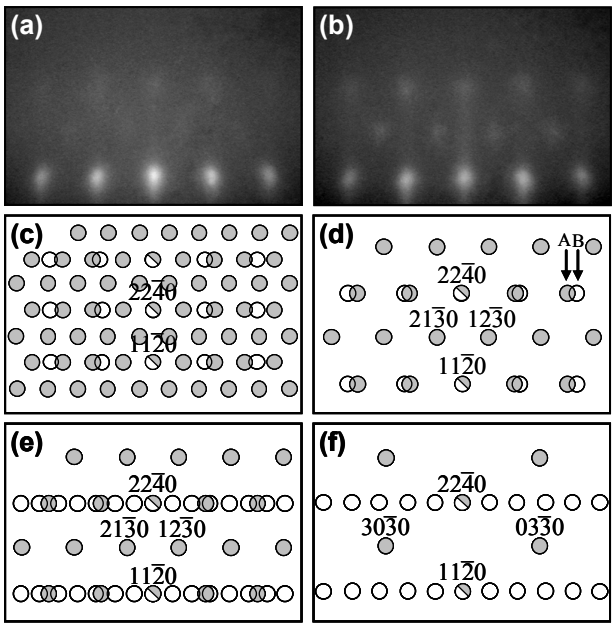

Fig. 1　(a, b) RHEED patterns observed during Sm-Co deposition on Cr(100) underlayer at 500 °C. The Sm-Co film thicknesses are (a) 5 and (b) 20 nm. (c–f) Schematic diagrams of RHEED patterns simulated for (11$\bar{2}$0) surfaces of (c) Sm_2Co_{17}, (d) $SmCo_5$, (e) Sm_2Co_7, and (f) $SmCo_3$ crystals.

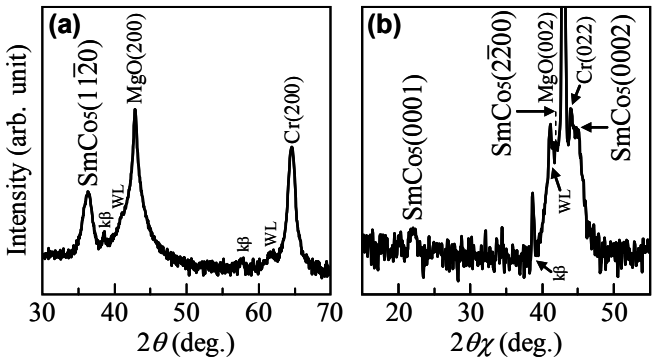

Fig. 2　(a) Out-of-plane and (b) in-plane XRD patterns of an Sm-Co film deposited on Cr(100) underlayer at 500 °C.

参考文献　1) E. E. Fullerton *et al.*: *Appl. Phys. Lett.*, **69**, 2438 (1996). 2) E. E. Fullerton *et al.*: *Appl. Phys. Lett.*, **71**, 1579 (1997). 3) M. J. Pechan *et al.*, *J. Appl. Phys.* **87** 6686 (2000).

Cu(111)下地層上におけるエピタキシャル RCo$_5$ 規則合金薄膜の形成

山田真・堀田裕介・鈴木中・大竹充・二本正昭・桐野文良*・稲葉信幸**
（中央大，*東京藝大，**山形大）

Preparation of Epitaxial RCo$_5$ Ordered Alloy Thin Films on Cu(111) Underlayers

Makoto Yamada, Yusuke Hotta, Ataru Suzuki, Mitsuru Ohtake,
Masaaki Futamoto, Fumiyoshi Kirino*, and Nobuyuki Inaba**
(Chuo Univ., *Tokyo Univ. Arts, **Yamagata Univ.)

はじめに　RCo$_5$（R：希土類元素）規則合金は 10^7～10^8 erg/cm^3 オーダーの高い K_u を持つものが多く，そのため，これらの薄膜は高密度磁気記録媒体などへの応用に向けて研究されている．これまで，Cu(111)下地層を用いることにより，磁化容易軸である c 軸が面直に向いた SmCo$_5$ 薄膜が形成されることが報告されている[1–3]．薄膜の基本構造や磁気特性を調べるためには，基板結晶に対して膜の結晶方位を制御できるエピタキシャルを用いることが有効である．しかしながら，SmCo$_5$ 合金膜以外の磁化容易軸が面直方向に向いたエピタキシャル RCo$_5$ 膜の形成例は殆ど報告されていない．本研究では，R 元素として，Y や Gd などを用いたエピタキシャル RCo$_5$ 膜の形成を試みた．

実験方法　薄膜作製には超高真空 MBE 装置を用いた．MgO(111)基板上に 20 nm 厚の RCo$_5$（at. %）（R = Y，Gd，など）合金膜を形成した．製膜時の基板温度を 500 °C とした．構造評価には RHEED および XRD を，磁化曲線測定には VSM を用いた．

実験結果　Fig. 1(a)に Y-Co 膜に対して観察を行った RHEED パターンを示す．形成初期過程から鮮明な回折パターンが観察されており，Fig. 1(b-2)に示す RT_5(0001)面の回折パターンと一致していることが分かる．このことからエピタキシャル YCo$_5$(0001)膜が形成されていることが確認された．また，Fig. 1(b-2)中の A，B に示すような異なる結晶方位関係を表す 2 つの回折パターンが重畳して現れている．よって作製した Y-Co 膜は双晶エピタキシャル膜であることが分かった．RHEED 解析から決定したエピタキシャル方位関係は以下の通りである．

$$YCo_5(0001)[11\bar{2}0],\ [1\bar{1}00] \parallel Cu(111)[11\bar{2}]$$

Fig. 2 に 20 nm 厚の Y-Co 膜から得られた面外 XRD スペクトルを示す．YCo$_5$(0002)基本反射に加え，YCo$_5$(0001)超格子反射が得られていることから，規則構造を持つ合金膜が形成されていることを確認できる．当日は，他の R 元素を用いた結果についても報告する．

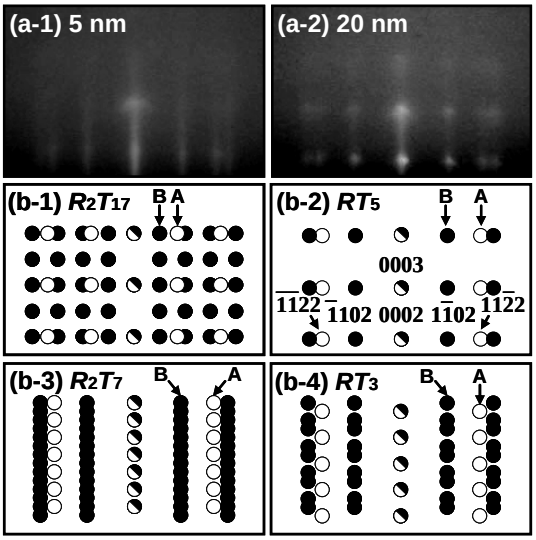

Fig. 1　(a) RHEED patterns of a Y-Co film observed during deposition on Cu(111) underlayer at 500 °C. The film thicknesses are (a-1) 5 and (a-2) 20 nm.
(b) Schematic diagrams of RHEED patterns simulated for (0001) surfaces with (b-1) R_2T_{17}, (b-2) RT_5, (b-3) R_2T_7, and (b-4) RT_3 ordered structure.

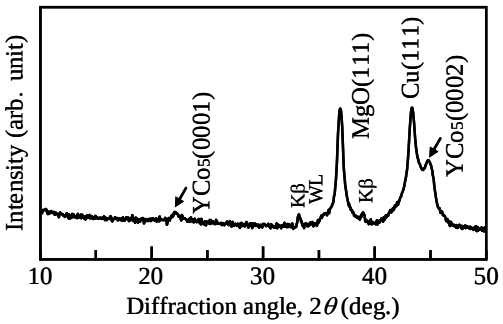

Fig. 2　Out-of-plane XRD pattern of a Y-Co film deposited on Cu(111) underlayer at 500 °C.

参考文献　1) S. Takei *et al.*: *J. Magn. Magn. Mater.*, **272–276**, 1703 (2004).　2) J. Sayama *et al.*: *J. Phys. D*, **37**, L1 (2004).　3) M. Ohtake *et al.*: *J. Cryst. Growth*, **311**, 2251 (2009).

ドロップレット低減による Sm-Co/α-Fe 積層型ナノコンポジット厚膜磁石の磁気特性改善

牧原峻佑、藤昭徳、柳井武志、中野正基、福永博俊

（長崎大学大学院　工学研究科）

Improvement in magnetic properties of PLD-made Sm-Co/α-Fe multi-layered nanocomposite film-magnets due to suppression of droplets

S. Makihara, A. Tou, T. Yanai, M. Nakano, H. Fukunaga

(Nagasaki University)

はじめに

Sm-Co/α-Fe ナノコンポジット磁石は高いキュリー温度、高い飽和磁化を有することから高温で使用される高性能磁石の候補として挙げられる[(1)]。我々は、600~800 層の積層構造（一層の厚み : 20~30nm）を有する等方性厚膜磁石を PLD 法を用いて作製し、室温において 100 kJ/m^3, 150℃において 60 kJ/m^3 の$(BH)_{max}$を有する磁石膜を報告した[(2)]。しかしながら、磁石膜にはドロップレットと呼ばれる微粒子が存在し、ナノオーダーの積層構造の妨げとなっていることが懸念される。

そこで本研究では、補助レーザを用いて Sm-Co/α-Fe 積層型ナノコンポジット磁石膜のドロップレットを低減し、その磁気特性を改善した。

実験方法

積層型ナノコンポジット磁石の作製には、$Sm_{1.9}Co_5$ 合金とα-Fe の複合ターゲット（面積比 1:1）を用いた。回転するターゲットに Nd.YAG レーザ（主レーザ : λ=355 nm）を照射し、対向する Ta 基板にターゲット物質を堆積させた。その際、ターゲットから放出されたドロップレットが基板に到達するのを防ぐため、主レーザに同期させた補助レーザを飛行するドロップレットに照射し（遅延時間 t_d）、ドロップレットを再アブレーションした(Fig.1)。成膜後、膜表面の SEM 観察及び平均表面粗さ R_a の測定により、ドロップレットの増減を定性的に評価した。

なお、成膜直後の Sm-Co 層は非晶質状態にあったので、パルス熱処理により磁気的に硬化させた。

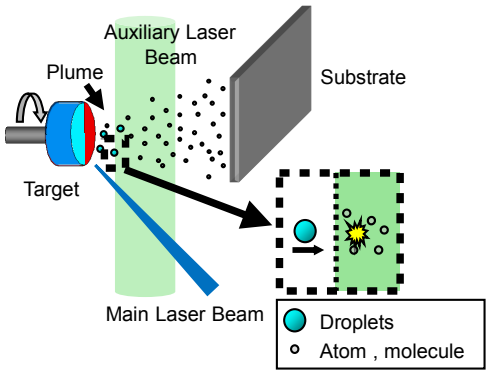

Fig.1 Experimental setup.

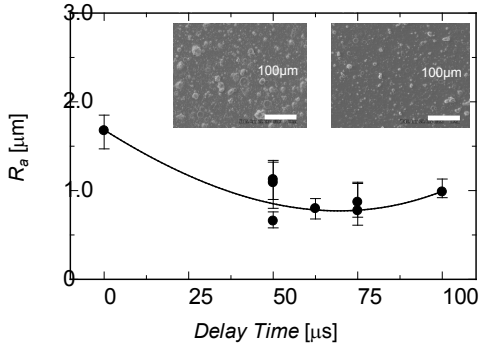

Fig.2 Average surface roughness R_a of Sm-Co/α-Fe multi-layered films as a function of delay time of auxiliary laser.

実験結果及び考察

Fig.2 に補助レーザの遅延時間 t_d に対する R_a の変化を示す。補助レーザを用いることで膜表面の平均粗さが小さくなることが了解される。このことは SEM 観察画像からも確認される。

Fig.3 に角型比を示している。補助レーザを使用することで角型比が向上している。これは、ドロップレットの抑制したことで、Sm-Co 層および α-Fe 層間の交換結合が有効に機能するようになったためと考えられる。

その結果、$(BH)_{max}$ は補助レーザを使用しないものに比べて約 10%向上し、H_c=357 kA/m, Jr=1.06 T, $(BH)_{max}$ =110 kJ/m^3 の特性が得られた。

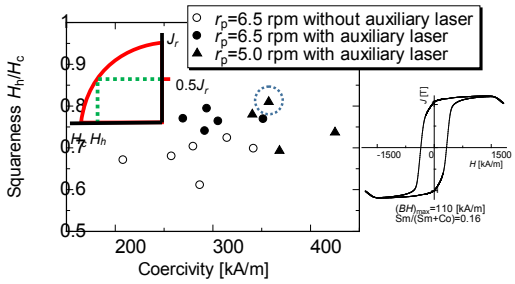

Fig.3 Squareness of demagnetization curve as a function of coercivity, together with hysteresis loop for the film shown by the dotted circle. The squareness is given by H_h/H_c which are defined in the inset.

参考文献

(1) H. Fukunaga et al., IEEE Trans. Magn. **49**, 3240 (2013).

(2) H. Fukunaga et al., IEEE Trans. Magn. **50**, 2101504 (2014).

アークプラズマ蒸着により作製したFe系ナノ粒子の磁気特性

松浦昌志，山本鉄郎，手束展規，杉本諭
（東北大学　大学院工学研究科）

Magnetic properties of Fe-based nano-particles prepared by arc-plasma deposition

M. Matsuura, T. Yamamoto, N. Tezuka, and S. Sugimoto
(Graduate school of Engineering, Tohoku University)

諸言

Fe系ナノ粒子はこれまで，液相法や気相法などの様々な方法を用いて作製されてきた．気相法の一種であるアークプラズマ蒸着法は金属ナノ粒子を作製する方法であるが[1]，さらに本手法は，金属ナノ粒子を基材となる粉末表面に担持させることが可能といった特徴を有している．しかしながら，本手法でFe系ナノ粒子を作製し，その磁気特性を調べた例はない．そこで本研究では，アークプラズマ蒸着法を用いて，安定酸化物であるSiO_2粉末にFe系粒子を堆積させたときの組織と磁気特性を調べた．

実験方法

試料は，到達真空度が $2x10^{-4}$ Pa以下のアークプラズマ蒸着装置を用いて作製した．ターゲットとしてFe-Co, Fe-Pt合金を用い，平均粉末粒径が70 nmのSiO_2粉末上に堆積した．なお，プロセスガスとしてAr+He混合ガスを用い，100~1000 ショットだけ堆積した．さらに，得られた粉末を 10^{-3} Pa以下の真空雰囲気下で熱処理した．得られた粉末を1.6 MA/mの外部磁場中で配向した後，6.4 MA/mのパルス磁場で着磁し，減磁曲線をVSMで測定した．粉末粒径ならびに結晶構造の評価は加速電圧が200 Vの高分解能TEMを用いて行った．

実験結果

Fig. 1に，SiO_2粉末上に堆積させたFe-Co系ナノ粒子のHR-TEM像を示した．Fig. 1より，SiO_2粉末上に，5~10 nmの粉末粒径を有するFe-Co系ナノ粒子がみられた．このことから，アークプラズマ蒸着法により，SiO_2粉末上に分散性よくFe-Co系ナノ粒子を作製することができた．このFe-Co系ナノ粒子の粉末粒径は，ショット数の増大に伴い大きくなる傾向がみられた．

Fe-Pt系についても同様の傾向がみられ，10~20 nm程度のFe-Pt系ナノ粒子がアークプラズマ蒸着により得られ，ショット数の増加に伴いその粒径が増大する傾向がみられた．制限視野回折(SAD)によりFe-Pt系粒子の構造解析を行った結果，熱処理により規則化が進行し，$L1_0$ FePt相が出現することが分かった．さらに，このFe-Pt系粉末の保磁力は熱処理に伴い増大することが明らかになった．

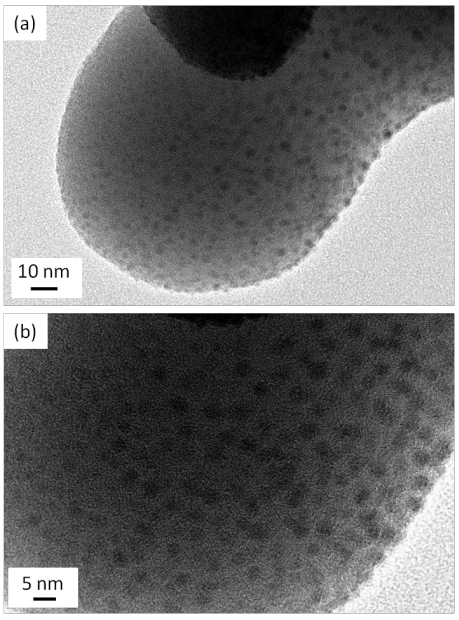

Fig. 1 HR-TEM images of Fe-based nano-particles prepared by arc-plasma deposition.

参考文献

[1]阿川ら，ULVAC TECHNICAL JOURNAL, 65 (2003) 1-5.

謝辞

本研究の一部は，学技術振興機構の戦略的創造研究推進事業（JST-CREST）ならびに，文部科学省の委託事業である元素戦略磁性材料研究拠点の支援の下で行われました．

$NdFe_{12}$、$NdFe_{12}N_x$ 薄膜の作製とその磁気特性評価

平山悠介、高橋有紀子、宝野和博
（物質・材料研究機構）

Preparation and magnetic properties of $NdFe_{12}N_x$ thin film

Y.Hirayama, YK.Takahashi, K.Hono
(The Elements Strategy of Initiative Center for Magnetic Materials, National Institute for Materials Science)

はじめに

R-Fe 系化合物（R : 希土類元素）には多くの相が存在するが、$ThMn_{12}$ 相は鉄の含有量が最大であるために、大きな磁化が期待される。また、希土類元素の含有量が少なく、資源の観点からも非常に有用な材料である。薄膜では $SmFe_{12}$ の合成に成功した例があるが [1]、バルクで $ThMn_{12}$ 構造を有する材料は、$R(Fe, M)_{12}$ のように Fe の一部を第三元素 M（Ti、Mo、V、W 等）に置換することで $ThMn_{12}$ 構造を保持できる [2]。$NdFe_{11}Ti$ は窒素を導入することで一軸異方性を示し、磁化は 1.38 T、異方性磁界は 8.0 T（@300K）、キュリー温度は 740 K であり [3]、高温では $Nd_2Fe_{14}B$ 磁石に匹敵する可能性を持つ。しかしながら、室温において保磁力は 1 T 以下に留まり、異方性磁界の約 1/10 程度である。高い保磁力を得るためには、保磁力機構の解明が必要不可欠であり、薄膜でのモデル磁石を用いた系統的な実験が求められる。そこで、本研究ではまず第三元素を添加せず、エピタキシャル $NdFe_{12}N_x$ 膜形成を目的として MgO(100)単結晶基板上に $NdFe_{12}N_x$ 膜の形成を試み、その結晶構造と磁気特性を評価した。

実験方法

試料作製には DC マグネトロン同時スパッタ法を用いた。600℃に加熱した MgO(100)基板上に下地層として W(001)をエピタキシャル成長させ、その上に約 70 nm の $NdFe_{12}$（at. %）膜を形成した。その後、15 mtorr の N_2 雰囲気下、400℃において 1 時間窒化処理を行うことで $NdFe_{12}N_x$ 膜を得た。構造評価には XRD (RIGAKU, SmartLab)、TEM（FEI, TitanG2）を、磁化曲線測定には VSM (Quantum Design, Inc. MPMS SQUID VSM)を用いた。

実験結果

Fig.1(a)に作製した試料の XRD 結果を示す。Fig.1(b)には chi、phi を適切に設定することにより得られた面からの回折ピーク示した。これらのことより、両試料で多少の α-Fe の析出は確認できるものの、c 軸が MgO(001)面に垂直であるエピタキシャル $NdFe_{12}$(N)の作製に成功した。さらに、これらの回折パターンより、格子定数はそれぞれ a = 0.852 nm、c = 0.480 nm（$NdFe_{12}$）、a = 0.849 nm、c = 0.492 nm（$NdFe_{12}N_x$）と算出され、窒素を導入することで体積が約 1.8%膨張したことがわかる。磁化測定結果より窒素を導入することにより、容易軸が ab 面から c 軸に変化し、一軸異方性を有する材料であることが確認できた。本発表では、詳細な磁化測定結果、TEM 観察結果も含めて報告する。

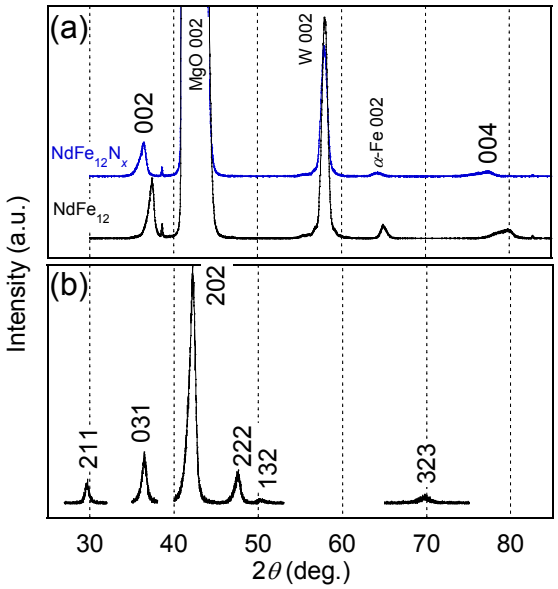

Fig.1 XRD spectra of $NdFe_{12}$ and $NdFe_{12}N_x$ (a) and obtained by setting the chi and phi appropriately in each plane of $NdFe_{12}$ film (b).

参考文献

1) Eric E. Fullerton *et al*., *Appl. Phys. Lett*. **69** (1996) 2438.
2) K H. J. Buschow, *J. Appl.Phys*. **63** (1988) 3130.
3) Ying-chang Yang *et. al*., *Solid State Commun.* **78** (1991) 317.

Coercivity enhancement of bulk hot-deformed Nd-Fe-B magnets by the eutectic grain boundary diffusion process using $Nd_{60}Dy_{10}Cu_{30}$ alloy

L. H. Liu [a,b], H. Sepehri-Amin [a], T. Akiya [a], T. Ohkubo [a], A. Hattori [c], K. Hioki [c], and K. Hono [a,b]
[a]National Institute for Materials Science, Tsukuba 305-0047, Japan
[b]Graduate School of Pure and Applied Sciences, University of Tsukuba, Tsukuba 305-8577, Japan
[c]Daido Steel Co., LTD, Nagoya 457-8545, Japan

Hot-deformed Nd-Fe-B magnets have high anisotropic microstructure composed of ultrafine grains that is comparable with single domain size of $Nd_2Fe_{14}B$ phase[1]. Coercivity, as extrinsic property, can be improved via modifications of grain boundary structure or its chemistry[2,3]. $(Nd,Dy)_2Fe_{14}B$ shell structure that forms after grain boundary diffusion has been considered as the reason of coercivity enhancement[4]. In this work, we applied low-temperature grain boundary diffusion to bulk hot-deformed Nd-Fe-B magnets using $Nd_{60}Dy_{10}Cu_{30}$ alloy powder to modify grain boundary composition and to enhance anisotropy field by localizing Dy at surface of $Nd_2Fe_{14}B$ grains.

Hot-deformed magnets with the composition of $Nd_{12.9}(Fe,Co)_{bal}\ B_{5.5}Ga_{0.5}$ (at.%) in 7×7×5.6 mm^3 size were used as the starting materials. The eutectic grain boundary diffusion was carried out by annealing at 650°C with sample coated with $Nd_{60}Dy_{10}Cu_{30}$ powder. The microstructures of the samples were studied using SEM/FIB (Carl ZEISS 1540EsB), TEM (Titan G2 80-200).

Demagnetization curves of the hot-deformed and diffusion-processed magnets of different heights are shown in Figure 1. The coercivity ($\mu_0 H_c$) of 5.6 mm, 5.8 mm, 6.0 mm high samples were enhanced from 1.4 T to 1.91 T, 2.15 T, and 2.26 T after diffusion process, respectively. The large slope of the demagnetization curves of diffusion-processed samples indicated coercivity distribution from surface to center. We find the formation of thicker intergranular phase with higher Dy segregation close to surface than that of the center region. STEM-EDS elemental maps showed micro-scale phase segregation of Nd and Nd-Dy-Cu (Fig.2). Formation of Nd-rich phase and $(Nd,Dy)_2Fe_{14}B$ shell at surface of $Nd_2Fe_{14}B$ grains are the main reasons for coercivity enhancement of diffusion-processed samples. Based on SEM and detailed TEM results, the mechanism of coercivity enhancement of bulk hot-deformed Nd-Fe-B magnets by grain boundary diffusion process will be discussed.

Reference

[1] R. W. Lee, E. G. Brewer, and N. A. Schaffel, IEEE Trans. Magn. **21**, 1958 (1985).
[2] H. Nakamura, K. Hirota, M. Shimao, T. Minowa, M. Honshima, IEEE Trans. Magn. **41** (2005), p. 3844
[3] H. Sepehri-Amin, T. Ohkubo, T. Nishiuchi, N. Zozawa, S. Hirosawa and K. Hono, Scripta Mater, **63**, 1124 (2010)

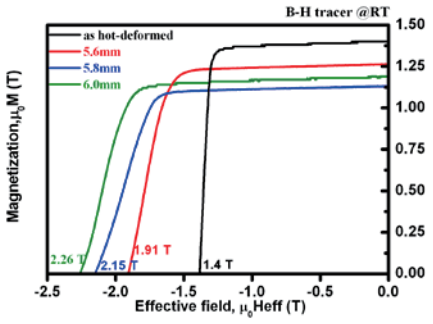

Fig.1 Demagnetization curves of hot-deformed and diffusion-processed magnets

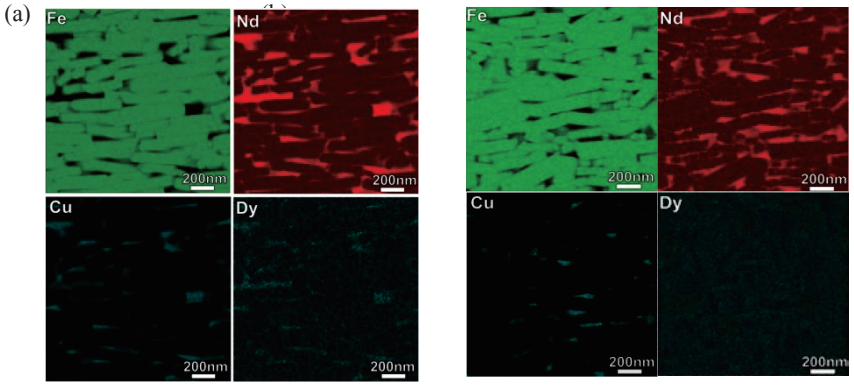

Fig.2 STEM-EDS mapping of surface region (a) and center region (b) of 6.0 mm high Nd-Dy-Cu diffusion-processed sample

Microstructure and Coercivity of Tb_4O_7 Grain Boundary Diffusion Processed Sintered (Nd,Dy)-Fe-B Magnets

U.M.R. Seelam[1], J. Liu[2], T. Ohkubo[1], H. Nakamura[3] and K. Hono[1,2]

[1]Elements Strategy Initiative Center for Magnetic Materials (ESICMM)
National Institute for Materials Science, 1-2-1 Sengen, Tsukuba, Ibaraki, Japan 305-0047
[2]Graduate School of Pure and Applied Sciences, University of Tsukuba, Tsukuba 305-8571, Japan
[3]Shin-Etsu Chemical Co. Ltd., Chiyoda, Tokyo 100-0004, Japan

In the grain boundary diffusion (GBD) process of Nd-Fe-B magnets, heavy rare earth elements (HREs) such as Dy and Tb are incorporated preferentially along the grain boundaries, instead of alloying them into the bulk. This results in a dramatic improvement in coercivity without losing remanence, leading to substantial savings in HREs.[1-3] However, it is well known that the alloying of Dy to the matrix is required to attain the coercivity higher than 2 T. In this study, a detailed microstructural characterization was carried out on terbium fluoride GBD processed (Nd,Dy)-Fe-B sintered magnets with four different Dy contents in order to understand the combined effect of Dy alloying and Tb GBD process. The nominal Dy compositions of the four base-alloys (prepared by two-alloy method) were 0, 2, 5, and 11 wt.%. Coercivity values of the four magnets before and after GBD process are, 1.2 and 1.9 T, 1.5 and 2.4 T, 2.1 and 3.2 T, and 3.6 and 4.3 T respectively. Microstructure of the four samples was characterized using scanning electron microscopy (SEM), electron probe micro analysis (EPMA), transmission electron microscopy (TEM) and atom probe tomography (APT). Figure 1 shows STEM/EDS mapping of Nd, Dy, Tb and Fe; average concentration (wt.%) of each element in the shells is shown next to it. Figure 2 shows high resolution STEM/EDS mapping of a grain boundary region containing shell. In addition to the Tb and Dy rich shell, a thin Nd-rich grain boundary phase is observed. The concentrations of Tb and Dy in the shell next to the grain boundary phase were estimated from the EDS analysis and correlated with coercivity. The coercivity after the GBD process is in accordance with the increase in the anisotropy field estimated from the concentration of Tb and Dy.

References

1) H. Nakamura, K. Hirota, M. Shimao, T. Minowa, M. Honshima, IEEE Trans. Magn. 41 (2005) 3844.
2) Z. Samardzija, P. McGuiness, M. Soderznik, S. Kobe, M. Sagawa, Mater. Charact. 67 (2012) 27.
3) H.S. Amin, T. Ohkubo and K. Hono, Acta Mater. 61 (2013) 1982.

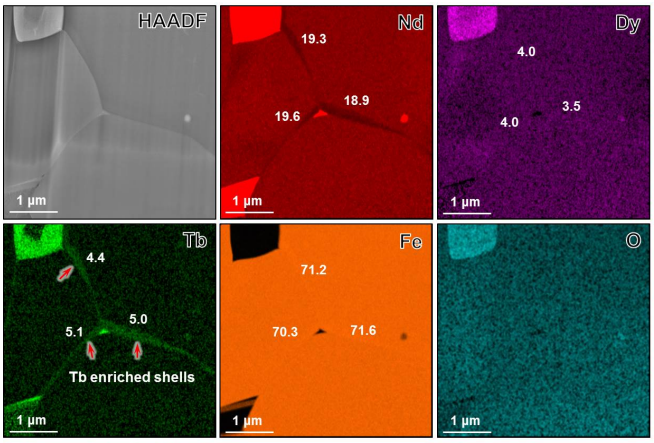

Figure 1. STEM/EDS mapping of Nd-5Dy-Fe-B sintered magnet showing Tb enriched shells

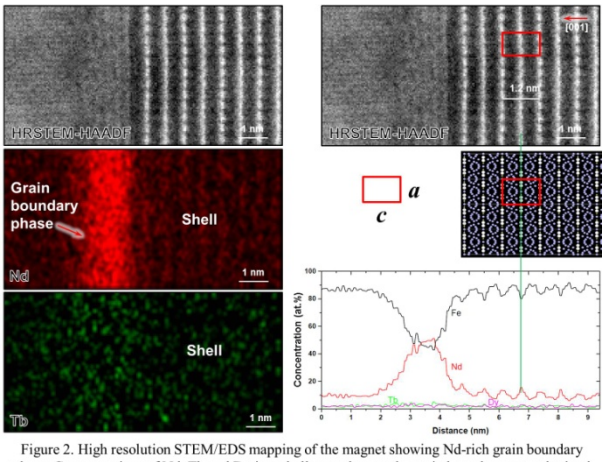

Figure 2. High resolution STEM/EDS mapping of the magnet showing Nd-rich grain boundary phase. Concentrations of Nd, Tb and Dy in a shell very close to the grain boundary were obtained

Nd-Fe-B 永久磁石における粒界相物性の焼結後熱処理温度依存性

保井晃、中村哲也、小谷佳範、深川智機*、西内武司*、広沢哲**
（JASRI/SPring-8、*日立金属、**物材機構）

Temperature dependence of post-sintered annealing on magnetic properties of intergranular phase in Nd-Fe-B permanent magnet

A. Yasui, T. Nakamura, Y. Kotani, T. Fukagawa*, T. Nishiuchi*, S. Hirosawa**
(JASRI/SPring-8, *Hitachi Metals, Ltd., **NIMS)

背景

Nd-Fe-B 永久磁石を製造する際に微量の Cu を添加し、焼結後に約 550℃で熱処理（アニール）を行うと保磁力が向上することが知られている[1]。これは、Nd/Nd-Cu の共晶反応により、粒界三重点に存在していた Nd-Cu を主とした物質が主相結晶間に薄く均一に広がり、主相結晶粒間の二粒子粒界相が幅約 3 nm に成長することで[2]、二粒子粒界相が磁壁の伝搬を阻害するピニングサイトとして働くためと考えられている。しかし、最適温度の 550℃を超えた温度でアニールした時に保磁力が減少傾向に転じる原因については、粒界相に何らかの変化があることが予想されるが、詳細は明らかになっていない。そこで、軟 X 線磁気円二色性(MCD)分光実験を用いて、粒界相における Fe および Nd 磁気モーメントと Cu 濃度を評価することで、アニール温度と保磁力および粒界相の物性との相関を調べた。

実験

測定試料は $Nd_{13.7}Fe_{78.0}B_{6.0}Cu_{0.1}$ 焼結磁石であり、組成分析の結果、O:1.4、C:0.5、Al:0.1、Si:0.1、N:0.1、Mn:0.02、Pr:0.02 (at%)が含まれていることが分かっている。それを石英ガラス管に真空封入し、1 時間アニールした後、石英管に封入した状態で外気に暴露し冷却した。アニール温度は、500℃、600℃、800℃、1000℃である。実験は SPring-8 BL25SU 電磁石 XMCD 装置を用いて行った。Nd-Fe-B 焼結磁石は粒界破断が支配的であるため、超高真空チャンバー(~5.0×10^{-7} Pa)内で試料を破断し、その破断面に対し軟 X 線 MCD 測定を行うことで、二粒子粒界相の物性を調べた。

実験結果

Fig. 1 に、$Nd_{13.7}Fe_{78.0}B_{6.0}Cu_{0.1}$ 焼結磁石の破断面における Cu L_3 吸収スペクトルのアニール温度依存性を示す。Cu 濃度は 500℃で最大をとり、それ以上のアニール温度では減少傾向に転じることが分かった。Fig. 1 の挿入図に示す通り、破断面での保磁力はバルクのそれと同様に最適アニール温度である 550℃付近で最大となり、粒界相の Cu 濃度と保磁力のアニール温度依存性の間に正の相関が見出された。

本研究の一部は、文部科学省の委託事業である元素戦略磁性材料研究拠点の支援を受けて行われました。

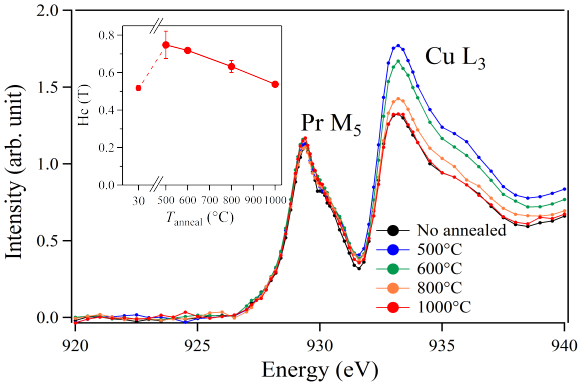

Fig.1: Annealing temperature dependences of Cu L_3 absorption spectra normalized with Fe L_3 absorption intensities. The inset shows coercivity of Fe-XMCD hysteresis curves measured on the fractured surface. This magnet contains Pr as an impurity.

参考文献

[1] 秋屋 貴博、加藤 宏朗、宇根 康裕、佐川 眞人，日本金属学会誌 第 76 巻，36 (2012).
[2] H. Sepehri-Amin, T. Ohkubo, T. Shima, K. Hono, Acta Materialia **60**, 819 (2012).

モータ駆動負荷による Nd-Fe-B 系焼結磁石の減磁評価

池田壮一郎、藤原幸星、森本祐治、竹澤昌晃、椛嶌寿行*
（九工大、*マツダ株式会社）

Evaluation of demagnetization of Nd-Fe-B sintered magnet by motor drive load

S. Ikeda, K. Fujiwara, Y. Morimoto, M. Takezawa, H. Kabashima*
(Kyushu Institute of Technology, *Mazda Motor Corporation)

はじめに

HEV、EV 等に用いられる永久磁石式同期モータの耐久信頼性を確保する上で、使用する磁石の耐減磁性能を正確に把握しておく必要がある。本研究では、Kerr 効果顕微鏡を用いてモータ用途を想定した形状の Nd-Fe-B 系焼結磁石をモータに搭載し、駆動前後の磁区構造変化を観察し、試料の位置による減磁特性の違いを明らかにすることを目的とした。そのために、観察結果に画像処理を施すことで、磁化反転領域を抽出し、各観察箇所における減磁率の算出を行ったので報告する。

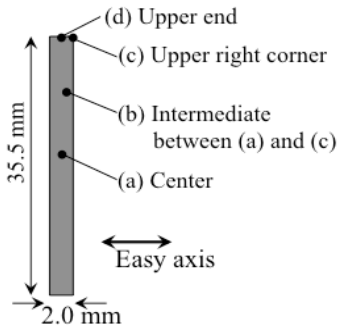

Fig. 1 Observed position.

実験方法

観察試料は、着磁方向である板厚が薄い Nd-Fe-B 系焼結磁石(幅 35.5 mm、長さ 40.5 mm、厚さ 2.0 mm)で、Dy は添加されておらず保磁力は約 11 kOe である。試料に合わせた研磨治具を作製し、着磁方向と平行な観察面を鏡面研磨した。磁区観察には縦 Kerr 効果顕微鏡を用いた。着磁した試料の残留磁化状態の磁区を観察した後、実際に試料を出力 1.5kW の IPM モータに搭載して 150℃まで加熱し、モータ駆動を行うことで試料に熱及び減磁界を与えた。その後、室温に戻した状態で再び磁区観察を行った。モータ駆動試験前後の磁区画像を比較し、磁化反転を起こした箇所を抽出し、その面積から減磁率の算出を行った。また、試料の位置による減磁率の違いを評価するために、Fig. 1 に示す(a)中央、(b) (a)と(c)の中間、(c)右上角、(d)上端の 4 点をそれぞれ観察し比較した。

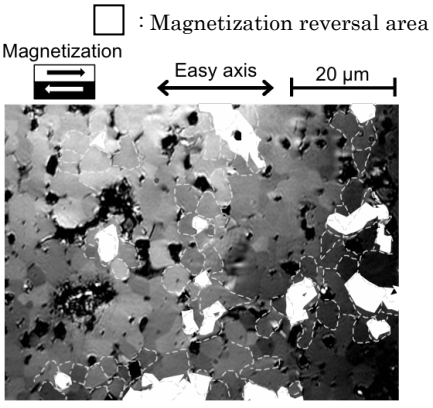

Fig. 2 Image processed magnetic domain image at center.

実験結果と考察

観察点(a)と(c)の磁化反転位置の観察結果を Fig. 2 と Fig. 3 にそれぞれ示す。図中の色付けを行っている領域が磁化反転を起こしている結晶粒である。Fig. 2 に示す中央において、モータ駆動により、多磁区構造をとらず粒全体で磁化反転する結晶粒が複数箇所で確認できた。磁化反転した部分の面積から減磁率の算出を行うと 18.7%となった。Fig. 3 に示す右上角では、磁化反転した結晶粒が Fig. 2 の場合より多く、減磁率は 40.6%であった。同様に減磁率を算出すると、(b)位置で 19.6%、(d)位置で 29.3%であった。これらの結果より、中央部から角部に近付くに連れて減磁率が高くなり、角部での減磁率は中央の約 2 倍大きくなることが分かった。モータ内の磁石周辺の磁気抵抗は、一様ではなく、磁石の両端部付近が、最も小さい。このため、磁石が受ける減磁界は、中央部よりも端部付近に集中する。よって、この減磁界強度の分布が、試料位置による減磁率の差異を生じさせたものと考えられる。これに加えて、本研究で用いた試料は、板厚が試料長さに比べ非常に薄いために反磁界が大きい。この反磁界は、中央部よりも端部で大きくなる。よって、この反磁界強度の違いが、端部と中央部との減磁率の差を拡大させた可能性があると推察する。

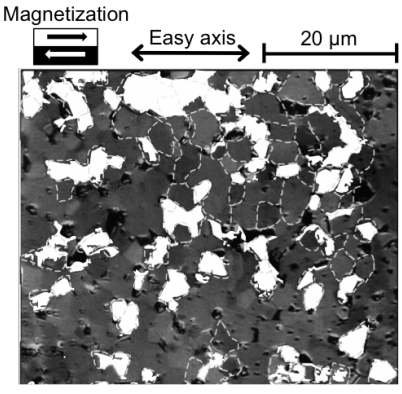

Fig. 3 Image processed magnetic domain image at upper right corner.

Synchrotron radiation analysis of structure and magnetism of grain boundary phase in Nd-Fe-B sintered magnet

T. Nakamura, A. Yasui, W. Ueno, N. Tsuji, T. Ohkubo[*], H. Iwai[*], T. Akiya[*], Y. Kotani, T. Fukagawa[**], T. Nishiuchi[**], Y. Gohda[***], K. Hono[*], and S. Hirosawa[*]
(JASRI/SPring8, [*]NIMS, [**]Hitachi Metals Ltd., [***]Univ. of Tokyo)

A high performance Nd-Fe-B permanent magnet has become an indispensable material for electric products, hybrid vehicles, and power generators, which are key technologies for energy sustainability. Associating with problem on the critical materials, improvement in coercivity without reduction of magnetization is intensely required in Dy-free type Nd-Fe-B magnets. Since it has been known that microstructure is essential for permanent magnets in order to increase the coercivity, the microstructure control may, therefore, bring a solution to developing the high performance Dy-free Nd-Fe-B sintered magnet. In a micro-magnetic point of view, a thin-film-like grain boundary (GB) phase existing between neighboring $Nd_2Fe_{14}B$ grains is preferred to be paramagnetic so as to prevent reversed magnetic domains from expanding into neighboring grains. Although the GB phase had been believed to be paramagnetic for a long time, the recent study using a three dimensional laser atom probe technique by Sepehri-Amin *et al*. showed convincing results indicating that the amorphous GB phase could be ferromagnetic [1]. Further studies on magnetism of the GB phase, however, are needed to uncover the origin of the coercivity.

In the present work, we have measured X-ray magnetic circular dichroism (XMCD) spectra in a $Nd_{14.0}Fe_{79.7}B_{6.2}Cu_{0.1}$ sintered magnet using synchrotron soft X-rays at BL25SU of SPring-8 in order to clarify the magnetic state of the GB phase. Since the Nd-Fe-B sintered magnets have a grain-boundary fracturing character, magnetism of the GB is directly investigated by the surface-sensitive XMCD measurement using a total electron yield (TEY) method [2]. The XMCD of the Fe $L_{2,3}$-edges was measured on the fractured surface which was covered with the GB phase. Applying the magneto optical sum rule [3-5], the apparent Fe magnetic moment was obtained as 1.66 μ_B from the XMCD spectra measured at 30 °C. Since the recorded XMCD signal was composed of those coming from the GB phase and the under-layered $Nd_2Fe_{14}B$ main phase, the magnetic moment of 1.66 μ_B was deconvoluted into each contribution on assumption of the probing depth of the TEY (λ_e=1.2 nm) at the Fe $L_{2,3}$-edges [2] and a thickness of the GB phase (t_B=3 nm) [1]. As the result of the deconvolution analysis, the Fe magnetic moment of the GB phase was estimated as 1.4 μ_B. This value is of about 60 % compared to that of $Nd_2Fe_{14}B$ and implies that the GB phase is ferromagnetic. Moreover, the temperature dependence of Fe magnetic moment in Fig. 1, which was obtained from the XMCD spectra, indicated that the Curie temperature of the GB phase was lower than that of the main phase, $Nd_2Fe_{14}B$. The present result, therefore, implies that the coercivity will possibly be improved by forming the GB phase which has the Curie point being lower than the operating temperature.

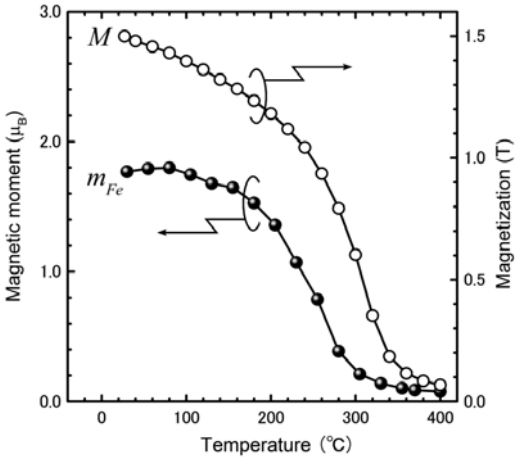

Fig. 1 Temperature dependence of Fe magnetic moments (m_{Fe}) obtained by sum rule analysis of XMCD spectra at the Fe $L_{2,3}$-edges and a magnetization (M). Both XMCD and magnetization were measured under 1.9 T.

It was reported that the thin-film-like GB phase grows by post-sintered annealing process [1]. The materials to form the GB phase could be supplied from somewhere like the Nd-rich phase at the triple junction during the annealing process. In order to elucidate the metallurgical phenomena with respect to the constitutional phases, we have investigated the crystal phases in the $Nd_{14.0}Fe_{79.7}B_{6.2}Cu_{0.1}$ sintered magnet by X-ray diffraction (XRD) experiment up to 1000 °C. High temperature *in-situ* XRD measurements were performed at BL02B2 of SPring-8. In

previous studies by means of transmission electron microscopy (TEM) [6, 7], it has been reported that the Nd-rich phase is a mixture of Nd ($P6_3/mmc$), Nd_2O_3 ($P6_3/mmc$), NdO_x ($Fm\bar{3}m$), and small amounts of other compounds, where symbols in parentheses denote the space groups of crystallography. Among them, the Nd-metal phase is expected to relate to the formation of the GB phase because the optimum annealing temperature of 540 °C is very close to the eutectic point of 520 °C in the Cu-Nd system. Fig. 2 shows temperature dependence of XRD patterns with labels denoting crystal phases determined by analysis of the XRD patterns. The Nd-metal phase ($P6_3/mmc$) starts melting at 580 °C (XRD pattern at 580 °C is not shown here), and completely melts at 606 °C. The melting point of the metallic Nd phase in the present experiment is higher than that expected from the eutectic point by 60 ~ 80 °C. This difference of the temperature is explained as that the XRD detects the crystalline Nd-metal unused in the eutectic reaction because the Cu concentration (0.1 at%) is too small to consume all of the crystalline Nd phases (>1 at%). Here, the volume fraction of Nd which exists as Nd metal was estimated from the Rietvelt analysis of XRD pattern. On the other hand, a different Nd phase having cubic crystal symmetry ($Fm\bar{3}m$) was also found in the temperature range between 335 ~ 788 °C. Variation in volume fraction of the cubic and hexagonal phases of Nd was invisible at the eutectic point. The Nd2O3 phase remains solid state even at 1000 °C, but shows some phase transitions with respect to crystal symmetries involving $P6_3/mmc$, $Ia\bar{3}$, and $P\bar{3}m1$. Although the mechanism of these phase transitions in the Nd_2O_3 phases is still not clear, the information may be useful in refining the Nd-O phase diagram which is important in elucidation of the microstructural formation mechanism of Nd-Fe-B magnets.

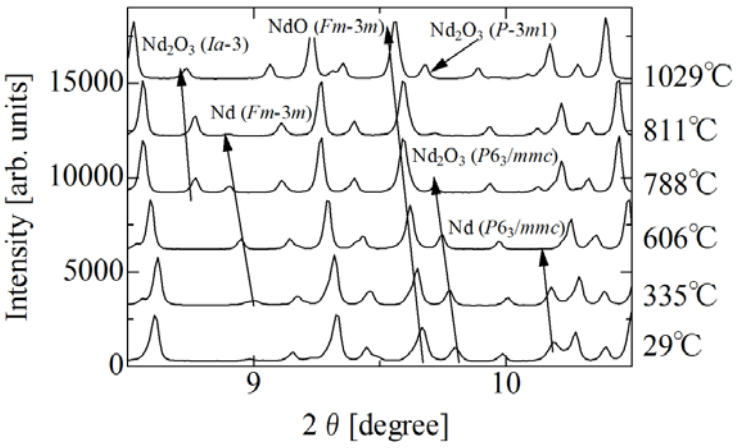

Fig. 2 Temperature dependence of XRD patterns of $Nd_{14.0}Fe_{79.7}B_{6.2}Cu_{0.1}$ sintered magnet. Arrows beside XRD peaks denote trends of shift of peak positions for identified crystalline phases.

Acknowledgements

The authors are grateful to Drs. J. Kim, K. Sugimoto, M. Suzuki, A. Fujiwara, and M. Takata of JASRI, and Dr. H. Sepehri-Amin and T. Abe of NIMS for fruitful discussions. A part of this work is supported by the Elements Strategy Initiative Center for Magnetic Materials under the outsourcing project of MEXT.

References

[1] H. Sepehri-Amin, T. Ohkubo, T. Shima, K. Hono, Acta Mater. **60**, 819 (2012).
[2] B. H. Frazer, B. Gilbert, B. R. Sonderegger, and G. De Stasio, Surf. Sci. **537**, 161 (2003).
[3] B. T. Thole, P. Carra, F. Sette, and G. van der Laan, Phys. Rev. Lett. **68**, 1943 (1992).
[4] P. Carra, B. T. Thole, M. Altarelli, and X. Wang, Phys. Rev. Lett. **70**, 694 (1993).
[5] C. T. Chen, Y. U. Idzerda, H. -J. Lin, N. V. Smith, G. Meigs, E. Chaban, G. H. Ho, E. Pellegrin, and F. Sette, Phys. Rev. Lett. **75**, 152 (1995).
[6] J. Fidler, IEEE Trans. Magn. **21**, 1955 (1985).
[7] Mo W, Zhang L, Liu Q, Shan A, Wu J, Komuro M. Scripta Mater. **59**, 179 (2008).

Effect of grain size reduction of Nd-Fe-B sintered magnet on temperature coefficient of coercivity.

Y. Une, H. Kubo, T. Mizoguchi, T. Iriyama, M. Sagawa, M. Nakamura※, M. Matsuura※, S. Sugimoto※
(Intermetallics Co., Ltd., ※Tohoku Univ.)

1. Introduction

Grain size reduction technique of Nd-Fe-B sintered magnets is well known process to increase a coercivity without substitution of Dy for Nd. We have been developing ultrafine grained Nd-Fe-B sintered magnets using a helium gas jet-mill which can produce smaller particle size of the powder than a conventional nitrogen gas jet-mill[(1)]. Recently, Nakamura *et al*.[(2)] have reported the development of single crystal powders with particle size of under 0.6 μm using a combination of HDDR (hydrogenation-disproportionation-desorption-recombination), hydrogen decrepitation, and the helium gas jet-mill processes. In the present study, we report magnetic properties of ultrafine-grained Nd-Fe-B sintered magnets with grain size of under 1 μm.

2. Experiment

The starting material in this study is the strip-cast (SC) alloy with the nominal composition of $Nd_{27.2}Pr_{4.23}FeB_{0.96}Cu_{0.1}Al_{0.24}Co_{0.95}Fe_{bal.}$(wt%). We prepared 3 kinds of powders with particle sizes of 3, 1 and <1μm. The 3 μm powders and the 1 μm powders were produced by using the nitrogen gas jet-mill and the helium gas jet-mill, respectively. For the <1μm powders, the SC alloys were performed the hydrogen decrepitation followed by HDDR treatment. Subsequently, the HDDR-treated alloys were crushed into ultrafine powders by using the helium gas jet-mill[(2)]. Each powder was filling into a carbon mold and subsequently was aligned with pulse magnetic fields of 5T. Then each powder in the molds was sintered at the optimum temperature in vacuum and annealed at optimum temperature. Magnetic properties were measured by B-H loop tracer from room temperature up to 180℃.

3. Results

Fig.1 shows the variation of the temperature coefficient of the coercivity (β) of the Nd-Fe-B sintered magnet vs a function of temperature interval (T-23℃). The temperature coefficient of the HcJ (β) of the magnets improves from -0.55 to -0.47 %/K between 23 and 180℃ with decreasing the particle size of the starting powders from 3 to under 1 μm.

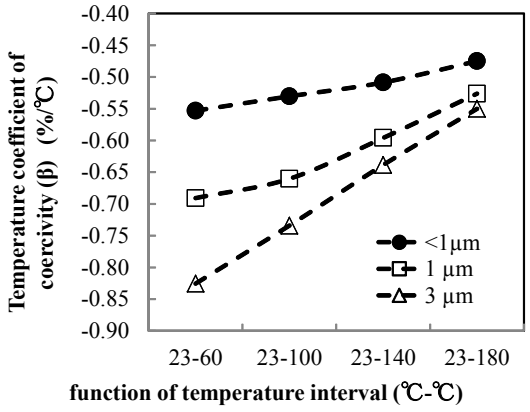

Fig.1 Variation of β of the Nd-Fe-B sintered magnet vs a function of temperature interval.

Reference

1) Y. Une and M. Sagawa, J. Jpan. Inst. Met. **76**, 12(2012) (in Japanese).
2) M. Nakamura *et al*., Appl Phys.Lett. **103**, 022404 (2013).

This study was supported by the "Future Pioneering Projects / Development of magnetic material technology for high-efficiency motors" from the New Energy and Industrial Technology Development Organization (NEDO) of Japan.

Low eutectic temperature alloy diffusion process for hot-deformed Nd-Fe-B magnet

T. Akiya[1], H. Sepheri-Amin[1], J. Liu[1,2], L. Liu[1,2], T. Ohkubo[1], K. Hioki[3], A. Hattori[3], K. Hono[1,2]
[1]Elements Strategy Initiative Center for Magnetic Materials, National Institute for Materials Science
[2]Graduate School of Pure and Applied Science, University of Tsukuba
[3]Daido Steel Co. Ltd.

Nd-Fe-B magnets have been studied for more than thirty years. One of main research issues of Nd-Fe-B magnet is low thermal stability due to its low Curie temperature (T_c ~ 310˚C). To improve the thermal stability, coercivity (H_c) enhancement is a possible way. For example, H_c of 3 T at room temperature (RT) is required for hybrid or pure electric vehicle and wind turbine generator to prevent a thermal demagnetization.

Coercivity of permanent magnet relates to the magnetocrystalline anisotropy field, H_a. The H_a of $Nd_2Fe_{14}B$ phase is about 7 T at RT and the value is theoretical maximum limit of coercivity. However, the coercivity of Nd-Fe-B magnet produced by conventional mass production route is only 1 T without Dy. It is accepted that the surface defects on $Nd_2Fe_{14}B$ particle and inclusions causes the degradation of coercivity, because the nucleation of reversed magnetic domain may occur at these sites. Here, $(Nd,Dy)_2Fe_{14}B$ phase possesses a higher magnetocrystalline anisotropy field than $Nd_2Fe_{14}B$. Therefore, Dy-rich shell structure formed by grain boundary (GB) diffusion process enhances the coercivity effectively with minimum amount of Dy for sintered magnet[1)].

It is empirically known that the coercivity of Nd-Fe-B magnet can be increased by refinement of $Nd_2Fe_{14}B$ crystals without Dy. A Nd-Fe-B sintered magnet with H_c ~ 2 T without Dy had been reported by Intermetallics Co.[2)]. They prepared fine $Nd_2Fe_{14}B$ powder with about 1 μm diameter by He-gas jet-milling technique. However, it is difficult to obtain sub-micron sized powder by jet-milling or any mechanical pulverization technique while preventing oxidation of the powders. Ultrafine $Nd_2Fe_{14}B$ crystal can be obtained by Hydrogenation-Decrepitation-Desorption-Recombination (HDDR) technique or die up setting process of rapidly quenched Nd-Fe-B alloy and then hot-deform processed magnet. These crystal sizes are one order of magnitude smaller than that of sintered magnet, about 300 nm in diameter particle (HDDR) and 300 nm in width and 50 nm in height of platelet shaped grain (hot-deformed), respectively. However, the reported coercivity of ultra-fine grain sized Nd-Fe-B HDDR powders and hot-deformed magnets is only around 1.5 T. This value is lower than expected from a trend of sintered Nd-Fe-B magnet, H_c ~ 2.5 T at 300 nm in diameter[3)].

We have studied the reasons of the low coercivity in three kind of Nd-Fe-B magnets, sintered[4, 5)], HDDR processed powder[6)] and hot deformed Nd-Fe-B magnet[7)]. In any case, the coercivity of Nd-Fe-B magnet relates to structure and chemistry of GB. It have been found that the GB of high coercivity magnet is thicker and contains lower Fe concentration[7)]. Fe-rich GB phase shows ferromagnetic property[5)], therefore, such ferromagnetic GB causes the magnetic coupling between $Nd_2Fe_{14}B$ grains. Thus, magnetic isolation between $Nd_2Fe_{14}B$ grains by nonmagnetic GB layer is critical point to enhance the coercivity.

We demonstrated that the low eutectic alloy diffusion technique is suitable way to modify the structure/chemistry of the grain boundary phase and enhance the coercivity in HDDR powder and hot-deformed magnet. This technique was independently reported by Sepehri-Amin *et al*.[6)] and Mishima *et al*.[8)] in the HDDR processed magnet powders. A low eutectic temperature alloy, such as Nd-Cu, Nd-Al and so on, infiltrates into GB rapidly in HDDR processed powder and hot-deformed magnet and thicker GB layer is formed between $Nd_2Fe_{14}B$ grains without significant grain growth. While, in sintered magnet, Cu diffuses into GB rapidly but the microstructure remains almost unchanged. Thus, the effect of Nd-Cu diffusion process is small in sintered Nd-Fe-B magnet.

Currently, we are focusing on the low eutectic temperature alloy diffusion process for hot deformed magnet. We have observed a coercivity enhancement from 1.5 T to 2.3 T using Nd-Cu eutectic alloy[9)], and 1.6 T to 2.6 T using

$Nd_{60}Dy_{20}Cu_{20}$ near-eutectic alloy[10] for small hot-deformed magnet with 1 mm thickness. While, remanence reduction of about 20 % was also observed due to infiltration of much amount of nonmagnetic material into magnet. After these works, we applied the technique to larger hot-deformed magnet with 5.6 mm thickness, and we confirmed that the infiltration effect occurs almost homogeneously and the coercivity enhancement occurs same as small specimen[11]. In addition, we observed sample expansion to mainly easy direction. The amount of diffusion alloy and volume expansion of magnet was almost comparable. So, we tried an expansion constraint method during diffusion process to prevent the excess diffusion of Nd-Cu phase[12]. As a result, we observed that the diffusion processed hot deformed magnet with constraint possesses higher remanence (M_r = 1.36 T) than simply diffusion processed one (M_r = 1.27 T). One of the reasons can be estimated that the diffusion processed magnet under constraint maintains the higher crystallographic texture than that of as hot-deformed and diffusion processed magnet without applying expansion constraint.

Temperature dependence of H_c and energy density [$(BH)_{max}$] of hot-deformed magnet and the samples that were Nd-Cu diffusion processed with and without an expansion constraint are shown in figure. For comparison, the energy densities of commercial 4% Dy and 8% Dy sintered magnets are also shown[13]. The temperature dependence of coercivity of Nd-Cu diffusion processed magnet is much better than original hot-deformed magnet and 4% Dy sintered magnet. This data suggests that the effect of ultrafine grain $Nd_2Fe_{14}B$ crystals appears by magnetic isolation in high temperature. In addition, the $(BH)_{max}$ of expansion constraint processed hot-deformed magnet is 358 kJ/m^3 at RT and 191 kJ/m^3 at 200 ˚C. This high-temperature property is slightly higher than that of Dy 4% sintered magnet.

We modified the GB of hot-deformed magnet by Nd-Cu diffusion technique. The amount of infiltrated nonmagnetic Nd-Cu into hot-deformed magnet was controlled by expansion constraint diffusion technique. As a result, we could obtain high coercivity as same as 4% Dy containing sintered magnet with high remanence. Obtained magnet possesses higher maximum energy product than 4% Dy containing sintered magnet at 200˚C without Dy. The next step of this work is to realize a magnet with H_c > 0.8 T and $(BH)_{max}$ > 150 kJ/m^3 at 200 ˚C.

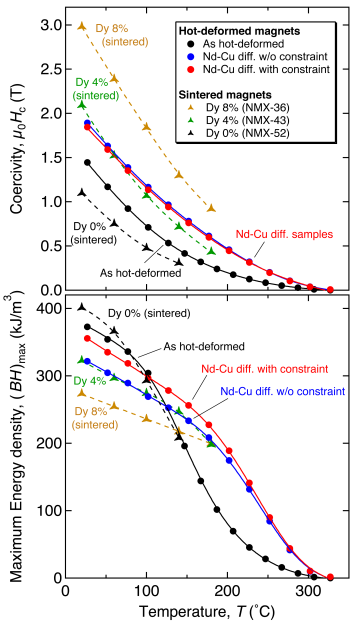

Fig. Temperature dependence of coercivity and maximum energy density.

References

1) H. Nakamura, K. Hirota, M. Shimao, T. Miniwa, M. Honshima, IEEE Trans. Magn. 41 (2005) 3844.
2) Y. Une, M. Sagawa, J. Japan. Inst. Metals, 76 (2012) 12-16.
3) K. Hono, H. Sepehri-Amin, Scripta Mater. 67 (2012) 503.
4) W.F. Li, T. Ohkubo, K. Hono, M. Sagawa, J. Magn. Magn. Mater. 321 (2009) 1100.
5) H. Sepehri-Amin, T. Ohkubo, T. Shima, K. Hono, Acta Mater. 60 (2012) 819.
6) H. Sepehri-Amin, T. Ohkubo, T. Nishiuchi, S. Hirosawa, K. Hono, Scripta Mater. 63 (2010) 1124.
7) J. Liu, H. Sepehri-Amin, T. Ohkubo, K. Hioki, A. Hattori, T Schrefl, K. Hono, Acta Mater. 61 (2013) 5387.
8) C. Mishima, K. Noguchi, M. Yamazaki, H. Mitarai, Y. Honkura. Proceedings of the 21st Workshop on Rare-Earth Permanent Magnets and their Applications, Bled, 29 August 2010, p. 253.
9) H. Sepehri-Amin, J. Liu, T. Ohkubo, K. Hioki, K. Hono, Scripta Mater. 69 (2013) 647.
10) H. Seprhri-Amin, T. Ohkubo, S. Nagashima, M. Yano, T. Shoji, A. Kato, T. Schrefl, K. Hono, Acta Mater. 61 (2013) 6622.
11) T. Akiya, J. Liu, H. Sepehri-Amin, T. Ohkubo, K. Hioki, A. Hattori, K. Hono, J. Appl. Phys. 115 (2014) 17A766.
12) T. Akiya, J. Liu, H. Sepehri-Amin, T. Ohkubo, K. Hioki, A. Hattori, K. Hono, Scripta Mater. 81 (2014) 48.
13) http://www.hitachi-metals.co.jp/products/auto/el/pdf/nmx.pdf

Magnetic domain structure observation of Dy free hot-deformed Nd-Fe-B magnets

Keiko Hioki, Atsushi Hattori, Takahiko Iriyama
(Daido Steel Co., Ltd.)

Nd-Fe-B magnets have a fine microstructure due to their unique fabrication procedure, which gives them 1/10 finer crystal grain size (100~500nm) compared to sintered magnets and produces both better coercivity and reduced Dy content[(1)]. However, the coercivity is not as high as expected from the grain size. To further improve the magnetic properties of this type of magnet, it is important to clarify the reason for the higher coercivity of this magnet. As the first step, we investigated the magnetic domain pattern structure of this magnet in detail.

A hot-deformed Dy-free Nd-Fe-B magnet with the composition of $Nd_{13.5}$-$Co_{3.82}$-$B_{5.64}$-$Ga_{0.57}$-$Fe_{bal.}$ (at.%) was prepared. Its remanence and coercivity were 1.35 T and 1353 kA/m (17.0 kOe), respectively. Observations for this sample were performed from two directions, perpendicular to the c-axis and almost parallel to the c-axis. In this study, the observations of the magnetic domains in the thermally magnetized state and in the magnetization process were performed. These observations were performed using not only Magnetic Force Microscope (MFM) and Atomic Force Microscope (AFM) but also Low Voltage Scanning Electron Microscope (LV-SEM) at the same areas, in order to investigate the relationship between the microstructure and magnetic domain pattern.

Figure 1(a) shows MFM images for the c-plane and (b) shows the illustration of magnetic domain pattern in the same area. Contours of grains observed using LV-SEM are overlaid in the figure. These figures reveal the following: 1. the sample consists of single domain and multi-domain grains, 2. a group of grains form a maze pattern, 3. multi-domain grains exist uniformly throughout the powder, and 4. relatively large grains at the edges of the maze pattern are multi-domain grains. In Fig. 1(c), magnetic domains looking at the plane parallel to the c-axis exhibited the stripe patterns parallel to the c-axis with various widths, some of which are interrupted by the equiaxial grains at powder boundaries. From these observations, the 3D magnetic domain structure of hot-deformed magnet is as portrayed in this figure.

Based on these observations, the magnetic domain structure of hot-deformed Nd-Fe-B magnets will be discussed.

Reference

1)　K. Hioki, A. Hattori, and, T. Iriyama, *J. Magn. Soc. Jpn.*, **38**, 79-82(2014)

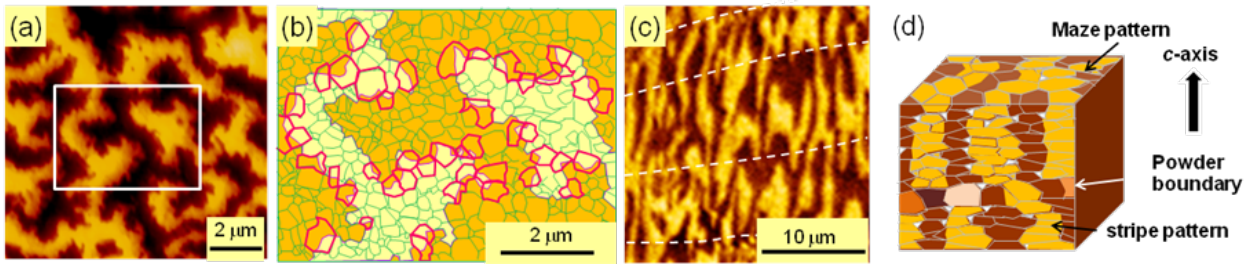

Fig. 1.　(a)(c) MFM images in the thermally demagnetized state. Looking at the planes (a) perpendicular and (c) parallel to the c-axis, respectively. Dotted lines indicate powder boundaries. (b) Illustration of magnetic domain pattern shown in Fig. 1(a) in the white square. Contours of grains observed using LV-SEM are overlaid. Multi-domain grains are shown in bold lines. (d) Illustrations of three dimensional magnetic domain structure of hot-deformed magnet in the thermally demagnetized state.

Observation of magnetic domain reversals in Nd-Fe-B hot-deformed and infiltrated magnets by SANS

M. Yano[1], T. Ueno[2], K. Saito[3], K. Ono[3], M. Harada[4], A. Manabe[1], T. Shoji[1], N. Sakuma[1], A. Kato[1], and U. Keiderling[5]

[1] Advanced Material Engineering Div., Toyota Motor Corporation, Susono 410-1193, Japan
[2]Elements Strategy Initiative Center for Magnetic Materials, National Institute for Materials Science, Tsukuba 305-0047, Japan
[3] High Energy Accelerator Research Organization (KEK), Tsukuba 305-0801, Japan
[4] Toyota Central R&D Labs. Inc., Nagakute 480-1192, Japan
[5]Helmholtz-Zentrum Berlin für Materialien and Energie, Berlin 14109, Germany

Nd-Fe-B magnet in motors in hybrid or electric vehicles requires Dy to increase its coercivity to maintain their magnetization in an operating temperature. However, Dy reduces magnetization in the magnet due to anti-parallel coupling of the magnetic moment between Dy and Fe [1]. To understand the coercivity mechanism in the Nd-Fe-B magnet to satisfy both high coercivity and magnetization, we have studied microstructures and magnetic domains in the magnet.

In general, the coercivity of Nd-Fe-B magnets can be enhanced by reducing the grain size of $Nd_2Fe_{14}B$ phase but it was found that only the grain size reduction cannot realize enough coercivity because of the reversal domain connections during demagnetizing procedures [2]. To reveal factors for higher coercivity, it is important to show the relation among magnetic properties, microstructures and magnetic domain reversals by using several kinds of methods because the microstructures and the magnetic domains are correlated to the coercivity.

Small-angle neutron scattering (SANS) is one of the complementary method to two-dimensional observations using microscope and it has a possibility to quantify the three-dimensional and multi-scaled microstructures and magnetic domains. The SANS enables us to investigate the bulk magnets using high transmission neutrons. Moreover, SANS can be performed under various sample environments of magnetic fields or temperatures.

In order to clarify the effect of grain isolation in nano-crystalline Nd-Fe-B magnets, we have prepared samples with different grain isolation and have performed SANS measurement to observe the difference in microstructures and magnetic domain reversals in these samples.

The hot-deformed Nd-Fe-B magnets have been made from rapidly quenched melt-spun ribbons. The melt-spun ribbons were crushed into a few hundred μm and then sintered at 873 K under a pressure of 100 MPa. The sintered bulk was hot-deformed with height reduction of about 80% to develop a (001) texture of phase. The hot-deformed magnet was soaked into the molten Re-Cu (Re=Pr or Nd) alloys to infiltrate into the grain boundaries to isolate grains [3]. The magnetic properties of as-deformed and Pr-Cu infiltrated samples are shown in Fig. 1 (a).

The SANS was performed at the V4 beamline of the research reactor BER-II at Helmholtz-Zentrum Berlin (HZB), Germany. The samples were fully magnetized along the easy magnetization axis ([001]-axis) at 10 T in advance. The sample temperature was set to 300 K. Neutron beam with the wavelength of 1.147 nm was used. Incoming beam direction was perpendicular to the [001]-axis and the irradiated area at the sample was set to 8 mm in diameter by the neutron window. The typical q range was 0.013–0.165 nm^{-1} with a sample-detector distance of 15.76 m. External magnetic fields of ± 5 T were applied along the [001]-axis to obtain magnetic field-dependent SANS patterns.

The magnetic field dependences of intensity I(q) along the [001]-perpendicular direction for as-deformed and Pr-Cu infiltrated samples are shown in Fig. 1 (b). Note that the scattering vector q and the dimension in real space d can be converted using Bragg equation, $d = 2\pi/q$. The variation of the intensities in a specific q-range corresponds to the variation of the microstructure or magnetic domains of the dimension d. As shown in Fig. 1 (b), the intensities increase by applying the reversal field for as-deformed sample and become maximum at the coercive field of $\mu_0 H_c = -1.46$ T. For

the infiltrated sample, intensities along the [001]-perpendicular direction also increase by applying the reversal field, as observed in the as-deformed sample, but the intensity difference is smaller. To magnify the magnetic field dependence as a function of the q or d, the intensity difference from that at 5 T are shown in Fig. 1 (c). The intensity difference becomes maximum at the coercive field of each sample. The intensity of smaller d range is dominant for as-deformed sample although the intensity of larger d range is dominant for infiltrated sample. These results indicate that the single particle reversal is dominant in the infiltrated sample implying that the larger ratio of the isolated grains than that of the interacting grains in the [001]-perpendicular direction, as compared to the as-deformed one.

These SANS results will be compared with the results of Nd-Cu infiltrated samples or direct magnetic domain observation by microscope.

Reference

[1] J. F. Herbst and W. B. Yelon, J. Appl. Phys. **57**, 2343 (1985).

[2] M. Yano *et al*., IEEE Trans. Mag., **48**, 2804 (2012).

[3] H. Sepehri-Amin *et al*., Acta Materia., **61**, 6622 (2013).

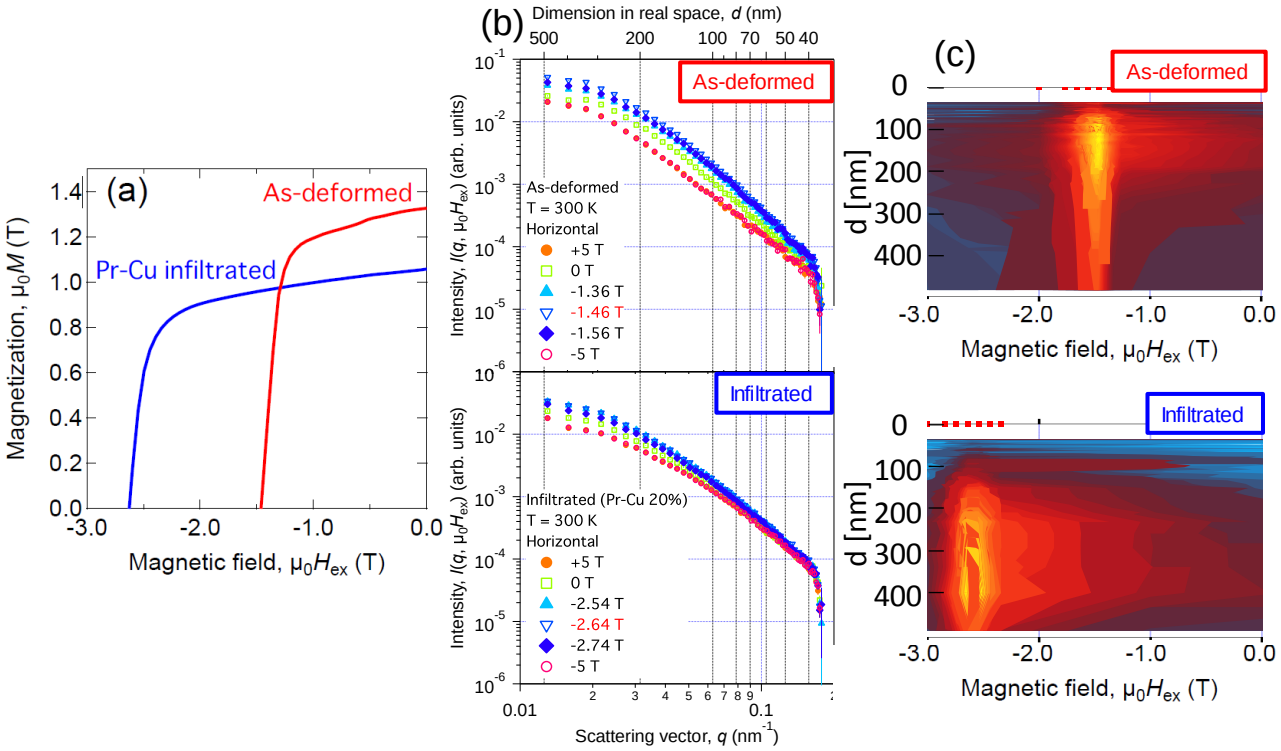

Fig. 1 (a) Demagnetization curves for as-deformed and Pr-Cu infiltrated Nd-Fe-B nano-crystalline magnets. (b) Magnetic field dependence of SANS intensities of as-deformed and infiltrated magnets. (c) Intensity difference between fully magnetized state and each demagnetization field. These intensity maps can be produced by (b).

Large-Scale Micromagnetic Simulation of Reversal Processes in Nd-Fe-B Magnets

A. Furuya[1], J. Fujisaki[1], K. Shimizu[1], T. Tanaka[1], T. Ataka[1], Y. Uehara[1], H. Oshima[2], T. Ohkubo[3], S. Hirosawa[3] and K. Hono[3]
[1]Fujitsu Limited, Kawasaki 211-8588, Japan
[2]Fujitsu Laboratories Limited, Atsugi 243-0197, Japan
[3]National Institute for Materials Science, Tsukuba 305-0047, Japan

Introduction:

Nd-Fe-B sintered magnets which have high maximum energy product and coercivity are widely used in electric motors and generators. To improve their properties, theoretical elucidation of the reversal process is demanded. In particular, the relationship between coercivity and their microscopic structures is an important topic for the improvement both from the scientific and technological points of view [1, 2]. To understand coercivity mechanism, theoretical studies based on micromagnetics have been performed to analyze the reversal process in Nd-Fe-B magnets. However, the edge length of numerical mesh element has to be smaller than the exchange length (1.7nm in Nd-Fe-B phase) in order to avoid “artificial pinning” in the simulation. Typically, grain size of sintered Nd-Fe-B magnets is from 100nm to 10μm. To simulate the pinning and nucleation process in the realistic grain structures, therefore, the number of finite elements involved in the numerical calculations exceeds a huge value of the order of millions. In this study, large-scale micromagnetic simulation is performed on K computer [3]. The effects of microstructure on the coercivity are numerically investigated.

Calculation methods:

We consider the following micromagnetic energy E_{tot} to analyze the magnetization in the simplified microstructure of Nd-Fe-B magnets,

$$E_{tot} = E_{Zeeman} + E_{exc} + E_{ani} + E_d , \tag{1}$$

where, E_{Zeeman}, E_{exc} , E_{ani} and E_d are Zeeman energy, exchange energy, anisotropy energy and magneto-static energy, respectively. The magnetization dynamics of the reversal processes are simulated by calculating the Landau-Lifshitz-Gilbert (LLG) equation,

$$(1+\alpha^2)\frac{\partial \boldsymbol{m}}{\partial t} = -\gamma\left(\boldsymbol{m}\times\boldsymbol{H}_{eff}\right) - \gamma\alpha\boldsymbol{m}\times\left(\boldsymbol{m}\times\boldsymbol{H}_{eff}\right), \tag{2}$$

where, m, γ and α are the normalized magnetization vector, the gyro-magnetic ratio, and the Gilbert damping factor. The effective field $\boldsymbol{H}_{eff}$ is derived from partial derivative of magnetization energies. The spatial distribution of the magnetization vector is numerically divided to the elements of the unstructured mesh which is commonly used in finite element method. To handle the domain wall motion and nucleation of the reverse domains, we used a small mesh size(1nm) and adapted the domain decomposition method by using METIS library, which divided the entire model in the small region and each region was calculated by the separate CPUs [4].

Simulations:

The simulation model is shown in Fig.1. This model is composed of 27 grains whose diameter is 50 nm. The grains are three-dimensionally aligned and the width of grain boundary is 2 nm. The total number of mesh model is about 5 million. We here label the state of a magnetic vector which points to positive y-direction “up”, and the opposite state “down”. As shown in Fig.1, all the initial magnetic vectors are down except for those in the grain of the front side of the top layer, which are initially in the up state. The simulated reversal process in the case of the alignment α=1 is shown in Fig.2. Due to the inclusion of the soft magnetic layers in the grain boundaries, the reversal domain easily propagates into neighboring grains. The simulation result at the alignment α=0.5 is also shown in Fig.3.

This result shows that the grain boundaries pin the domain wall of initial reverse domain and the nucleation occurs at another grains. The reversal mechanism depends on the microstructure and material parameters of the grain boundaries. In the presentation, the parameter dependences of the reversal processes and coercivity will be reported in detail.

Acknowledgment

This research used computational resources of the K computer provided by the RIKEN Advanced Institute for Computational Science through the HPCI System Research project (Project ID: hp120086).

References

1) Y. Matsuura; Proc. of the 22nd REPM (2012) pp.147-150
2) H. Sepehri-Amin, T. Ohkubo, T. Shima, and K. Hono, Acta Mater. 60, 819 (2012).
3) http://www.aics.riken.jp/en/kconmuputer/ ,Homepage of RIKEN Advanced Institute for Computatonal Science
4) G. Karypis and V. Kumar. SIAM Journal on Scientific Computing, 20 (1999) 359

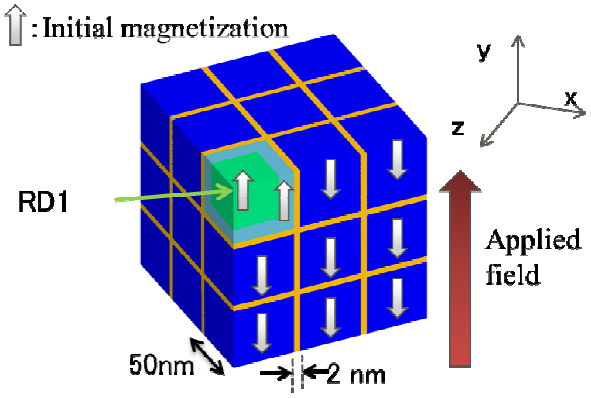

Fig. 1 Simulation Model of multi-grain structure

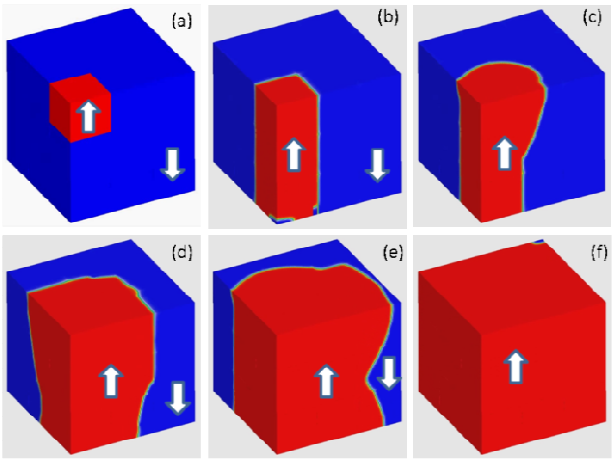

Fig. 2 Contour plot of m_z in the case of alignment parameter α=1.

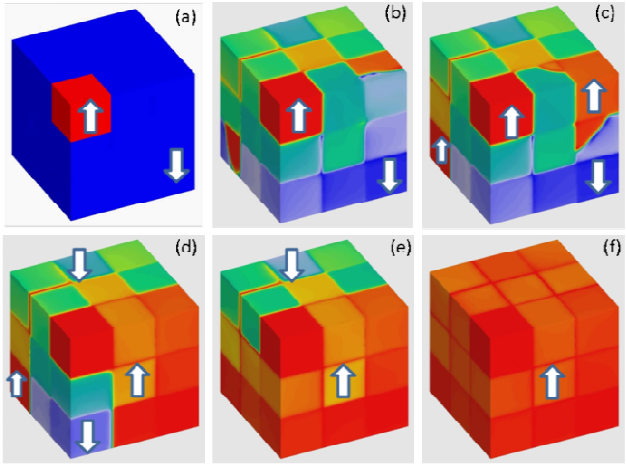

Fig. 3 Contour plot of m_z in the case of alignment parameter α=0.5

Anisotropy inducement mechanism in hydrogen disproportionation desorption recombination (HDDR) processed Nd-Fe-B powders

H. Sepehri-Amin[1], T. Ohkubo[1], K. Hono[1], K. Güth[2], and O. Gutfleisch[2,3]

[1]Elements Strategy Initiative Center for Magnetic Materials, NIMS, Tsukuba, Japan
[2]Fraunhofer ISC Projektgruppe IWKS, Germany
[3]Materialwissenschaft, Technische Universität Darmstadt, Germany

Introduction

The hydrogenation-disproportionation-desorption-recombination (HDDR) process is an attractive and unique method for producing anisotropic nanocrystalline Nd-Fe-B powders. In order to develop highly textured Nd-Fe-B powders, HDDR process parameters need to be carefully chosen and controlled [1]. Although lots of investigations have been carried out to understand the mechanism of the anisotropy development in HDDR powders [1-3], some questions still remain. In this work, the microstructures of Nd-Fe-B powders that were HD processed at different hydrogen pressure (P_{H2}^{HD}) were investigated to fully clarify the mechanism of the anisotropic microstructure evolution.

Experimental

Dynamic hydrogenation disproportionation (HD) desorption recombination (DR) process was carried out on $Nd_{12.8}Fe_{80.1}B_{6.6}Ga_{0.3}Nb_{0.2}$ alloy powders at different HD hydrogen pressure, P_{H2}^{HD} = 30 kPa and 100 kPa. The microstructures of the samples in early stages of the HD process, a fully HD process, and an early DR process were investigated using SEM/FIB (Carl Zeiss 1540EsB), TEM (Titan G2 80-200), and a locally built laser-assisted three dimensional atom probe (3DAP) to characterize the memory sites responsible for the texture development.

Results

A high remanent magnetization of 1.43 T was obtained for the fully HDDR processed powder with P_{H2}^{HD} = 30 kPa, indicating a strong [001] crystallographic texture. However, P_{H2}^{HD} = 100 kPa led to weakly textured Nd-Fe-B powders with a remanent magnetization of 0.89 T.

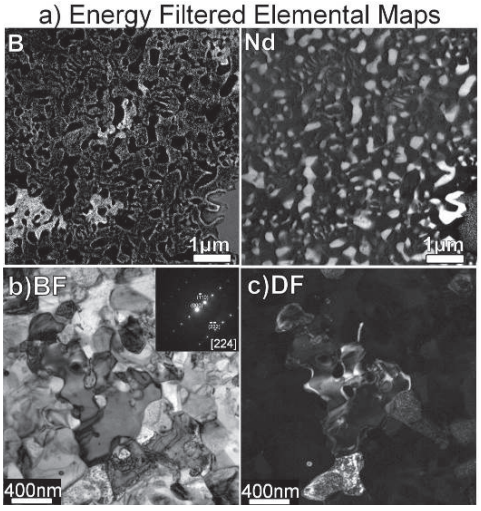

Fig. 1: (a) Energy filtered B and Nd maps of fully HD processed sample at P_{H2}=30kPa. (b) BF and (c) DF TEM images from the same sample indicating well textured Fe_2B grains. SADP obtained from a Fe_2B grain is shown in inset of (b).

TEM observations from early HD processed powder with P_{H2}^{HD} = 30 kPa showed that the Fe_2B phase has a direct crystallographic orientation relationship with the initial $Nd_2Fe_{14}B$ grains, i.e. $[420]_{Fe2B}||[211]_{Nd2Fe14B}$ and $(00\bar{2})_{Fe2B}||(\bar{1}\,11)_{Nd2Fe14B}$. Energy filtered (EF)-TEM and 3DAP results obtained from a fully HD processed sample showed boron not only in the Fe_2B phase but also at the NdH_2/α-Fe interfaces in both weakly and highly textured samples. High resolution STEM-HAADF image and nano-beam diffraction analysis from NdH_2/α-Fe interfaces showed that boron enrichment at these interfaces does not make a separate phase, such as iron boride. However, there is boron enrichment more in Fe grain of the NdH_2/α-Fe interface in nano-scale. Fig. 1(a) shows EF-TEM maps of B and Nd for the fully HD processed sample with P_{H2}^{HD} = 30 kPa. Bright field (BF)-TEM images obtained from the fully HD processed samples with different P_{H2}^{HD} showed that the Fe_2B regions in both

weakly and highly textured samples comprise of several small Fe_2B grains. Fig. 1 (b) and (c) shows BF and dark field (DF)-TEM images obtained from fully HD processed P_{H2}^{HD}=30 kPa sample. The DF-TEM image shows that the Fe_2B sub-grains in boride region of fully HD processed P_{H2}^{HD} = 30 kPa sample is strongly textured. Fig. 2 (a) shows BF-TEM image taken from the sample fully HD processed at P_{H2}^{HD} = 100 kPa. Superimposed EF-TEM maps of Nd (red), Fe (Blue), and B (green), obtained from the same region as Fig. 2(a), is shown in Fig. 2 (b). By comparing Fig. 2 (a) and (b), NdH_2, α-Fe, and Fe_2B phases can be distinguished. Selected area diffraction patterns obtained from different Fe_2B grains in boride area are shown in Fig. 2(c), indicating that the Fe_2B grains in the boride area are not well aligned in the sample fully HD processed at P_{H2}^{HD} = 100 kPa. Orientation relationship study of P_{H2}^{HD} = 30 kPa sample at early DR processed stage showed that recombined $Nd_2Fe_{14}B$ grains have direct orientation relationship with the remaining Fe_2B phase from HD process. In addition, 3D SEM tomography obtained from 3D serial sectioning of BSE images from P_{H2}^{HD} = 30 kPa sample at very early stage of DR process showed that the recombined $Nd_2Fe_{14}B$ grains nucleate at the interface of Fe_2B/NdH_2 grains and grow through the interface of NdH_2/α-Fe grains.

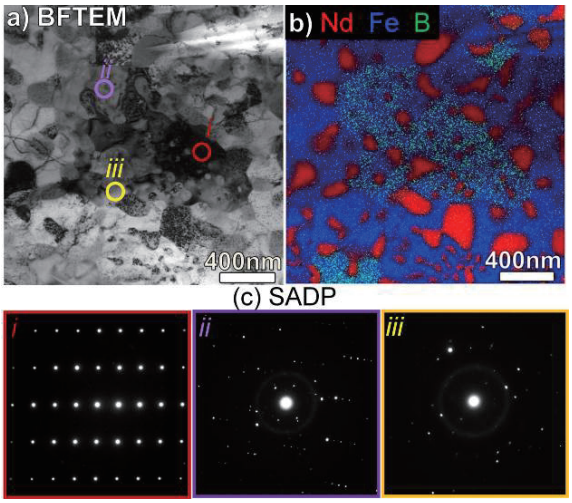

Fig. 2: (a) Bright field TEM image and (b) superimposed energy filtered Nd, Fe, and B maps of fully HD processed sample at P_{H2}=100kPa. (c) Selected area diffraction patterns obtained from different Fe_2B sub-grains in boride region.

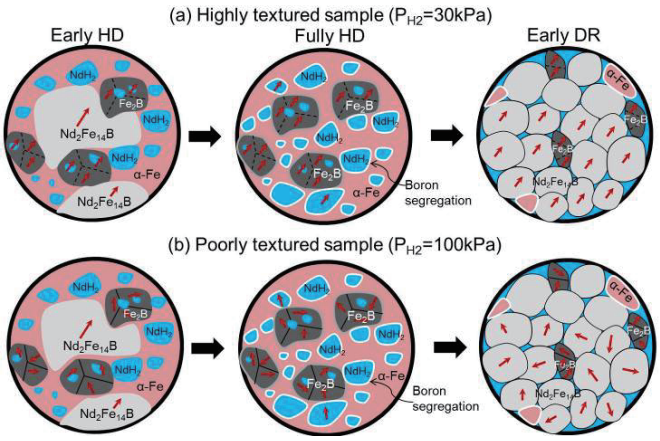

Fig. 3: Schematic illustration of microstructure evolution of HDDR processed sample with (a) P_{H2}^{HD} = 30 kPa (b) P_{H2}^{HD} = 100 kPa. This figure shows that in the highly textured powder, highly aligned Fe_2B grains act as memory sites and remembering the crystallographic orientation of initial $Nd_2Fe_{14}B$ grains and transferring the same orientation to the recombined $Nd_2Fe_{14}B$ grains.

These microstructure investigations indicate that the highly aligned Fe_2B grains act as memory sites for the development of the texture in the sample HD processed at P_{H2}^{HD} = 30 kPa, as shown schematically in Fig. 3, consistent with the previously proposed texture memory effect (TME) model. Importantly, it can now be shown that the recombined $Nd_2Fe_{14}B$ phase nucleates at the interface of Fe_2B with NdH_2 phase and grow through the interface of NdH_2/α-Fe interfaces and boron segregated at the NdH_2/α-Fe interface acts as a boron source for the growth of the recombined $Nd_2Fe_{14}B$ grains during DR process.

Reference

[1] O. Gutfleisch et al. IEEE Trans. Magn. 39 (2003) 2926.
[2] T. Tomida et al. Acta Mater. 47 (1999) 875.
[3] Y. Honkura et al. JMMM 290-291 (2005) 1282.